Journal of Energy Storage 86 (2024) 111432

Contents lists available at ScienceDirect

Journal of Energy Storage

journal homepage: www.elsevier.com/locate/est

Research papers

$In_{51}Bi_{32.5}Sn_{16.5}@SiO_2$ microcapsules-based composite phase change materials with high thermal conductivity and heat storage density for electronics thermal management

Chao Deng [a], Xinfeng Zhang [a], Jiale Peng [a], Xuan Yang [a], Bofeng Shang [b,*], Xiaobing Luo [a,*]

[a] School of Energy and Power Engineering, Huazhong University of Science and Technology, Wuhan 430074, China
[b] School of Physics and Microelectronics, Zhengzhou University, Zhengzhou 450001, China

ARTICLE INFO

Keywords:
Composite phase change materials
Microcapsules
Low melting point alloy
Thermal management
Thermal conductivity

ABSTRACT

Combining phase change microcapsules and various matrix materials can construct novel composite phase change materials (CPCMs). These composite materials hold immense potential for electronics thermal management, owing to their adjustable heat storage capacity and stable shape. Most previous studies focus on enhancing the thermal conductivity of CPCMs by adding thermally conductive fillers or modifying the microcapsule shells. Nevertheless, achieving both high thermal conductivity and heat storage density simultaneously remains a challenge. In this paper, low melting point alloy ($In_{51}Bi_{32.5}Sn_{16.5}$) was introduced as core material of the microcapsule to enhance the thermal conductivity, due to its significantly higher thermal conductivity compared to commonly used organic or inorganic phase change materials (PCMs). $In_{51}Bi_{32.5}Sn_{16.5}@SiO_2$ microcapsule was synthesized through the sol-gel polymerization method. Furtherly, a form-stable CPCMs consisting of the microcapsules and silicone rubber (SR) matrix were prepared for electronics thermal management. The $In_{51}Bi_{32.5}Sn_{16.5}@SiO_2$ microcapsules exhibit an impressive thermal conductivity of 13.49 Wm^{-1} K^{-1}, acting as a dual-functional filler for thermal storage and thermal conduction enhancement. Hence, the CPCMs possess a significantly enhanced thermal conductivity of 0.45 Wm^{-1} K^{-1}, representing a remarkable improvement of 350 % compared to that of pure SR. In addition, the phase change heat storage density of the CPCMs was as high as 71.73 J/cm^3. Notable, the prepared CPCMs demonstrate exceptional heat dissipation performance, resulting in a remarkable 23 °C reduction in chip temperature when applied for thermal management. This study offers a novel perspective on the preparation of microcapsule-based CPCMs for electronics thermal management.

1. Introduction

In recent years, electronic devices have been developing towards higher performance and integration [1,2]. The reduction in feature size leads to an increase in heat flow density of the chip, and the accumulation of heat causes over-temperature conditions that impact reliability and performance [3–5]. Therefore, effective thermal management is essential for ensuring stable operation of electronic devices. Compared with active cooling techniques such as forced air cooling or liquid cooling, passive cooling techniques using phase change materials (PCMs) possesses the advantages of low cost, high integration and high reliability which have garnered increasing attention [6–9]. PCMs can absorb or release large amounts of heat during the phase change process without a distinct temperature change themselves, exhibiting great prospective applications in energy storage and thermal management [10–13]. Based on the type of phase change process, PCMs are classified as liquid-gas, solid-gas, solid-liquid and solid-solid PCMs [14–16]. Among them, solid-liquid PCMs are currently the most commonly utilized due to their large latent heat, appropriate phase change temperature and wide variety available. Nevertheless, leakage problems during the phase transition process limits their scope of application [7,17–20].

Microencapsulation technology is considered an effective method to solve the leakage issues by encapsulating PCMs as core within the shell, forming microencapsulated phase change materials (MEPCMs) [21,22]. The shell of MEPCMs consists of both organic material such as melamine-formaldehyde (MF) [23], polystyrene (PS) [24], poly (ethyl-

* Corresponding authors.
E-mail addresses: shangbofeng@zzu.edu.cn (B. Shang), luoxb@hust.edu.cn (X. Luo).

https://doi.org/10.1016/j.est.2024.111432
Received 27 November 2023; Received in revised form 4 February 2024; Accepted 20 March 2024
Available online 23 March 2024

2-cyanoacrylate) (PECA) [25], as well as inorganic materials like SiO_2 [26,27] and TiO_2 [28]. Compared to organic shells, inorganic shells exhibit superior stability and higher thermal conductivity. Actually, MEPCMs cannot be directly utilized due to their powder form [29,30]. Hence, MEPCMs are combined with various matrix materials to prepare composite phase change materials (CPCMs), which expands their application field for thermal management in electronic devices [31–33], batteries [34–36], buildings [37,38] and smart textiles [39–41]. However, CPCMs incorporating microcapsules as functional fillers suffer from low thermal conductivity due to the low thermal conductivities of available MEPCMs.

Thermally conductive fillers were introduced into the polymer matrix to improve thermal conductivity in previous studies. Ma et al. [32] synthesized a series of composite materials by incorporating the MEPCMs, multi-walled carbon nanotubes and hexagonal boron nitride (h-BN) in polymer matrix. The thermal conductivity was improved to 0.44 Wm^{-1} K^{-1} with 3 wt% multi-walled carbon nanotubes and 10 wt% h-BN, which was 95.5 % higher than pure polymer matrix. Kang et al. [36] reported a phase change composite consisting of microcapsules and graphene sheets embedded in silicone rubber (SR). The thermal conductivity of composite materials was improved to 2.69 Wm^{-1} K^{-1} with the addition of 30 wt% graphene sheets. Liao et al. [29] prepared a composite material based on steric acid@SiO_2 phase change microcapsules and surface-modified boron nitride (m-BN). With the incorporation of 28 wt% m-BN, the thermal conductivity of the CPCMs reached 0.506 Wm^{-1} K^{-1}. Unfortunately, the introduction of thermally conductive fillers inevitably leads to a decrease in volume latent heat for CPCMs.

In order to avoid reducing the heat storage density when utilizing thermally conductive fillers, the most direct and effective approach is to enhance the thermal conductivity of microcapsules. Yuan et al. [42] prepared paraffin@SiO_2/GO microcapsules with a remarkable thermal conductivity of 1.162 Wm^{-1} K^{-1}, which was 13 % improvement than that of paraffin@SiO_2. Feng et al. [43] synthesized spherical paraffin@modified graphene-oxide particles with a core-shell structure by emulsion method, which presented a high thermal conductivity of 1.662 Wm^{-1} K^{-1}. It should be noted that the thermal conductivity of microcapsules remains relatively low despite potential further enhancements in the thermal conductivity, primarily due to their typically low shell-core ratio. Therefore, the primary solution to this issue is to enhance the thermal conductivity of the internal phase change heat storage core. Compared to common paraffin PCMs, the low melting point alloy possesses higher thermal conductivity and heat storage density, which can effectively enhance the overall thermal conductivity of microcapsules [44,45]. In addition, the phase change properties can be tailored by adjusting proportion of various metallic constituents [44,46]. As a result, the utilization of alloy microcapsules not only enable efficient heat storage, but also facilitates thermal conductivity enhancement by serving as thermally conductive fillers. In this way, simultaneous enhancement of thermal conductivity and thermal storage of the composite material can be realized.

In this work, low melting point alloy $In_{51}Bi_{32.5}Sn_{16.5}$ was selected as the core material due to its suitable phase change temperature of 60 °C. $In_{51}Bi_{32.5}Sn_{16.5}$@$SiO_2$ MEPCMs were synthesized through the sol-gel polymerization method. The morphology, chemical compositions, phase change properties, and thermal conductivities of the prepared MEPCMs were systematically characterized. Subsequently, the CPCMs were prepared by incorporating these microcapsules into the SR matrix, and their thermal conductivity and latent heat were measured. Finally, the heat dissipation performance of the CPCMs was evaluated. The CPCMs composed of SR and $In_{51}Bi_{32.5}Sn_{16.5}$@$SiO_2$ microcapsules with high thermal conductivity and heat storage density would be an efficient approach for the electronic thermal management.

2. Experiment

2.1. Materials

Low melting point alloy $In_{51}Bi_{32.5}Sn_{16.5}$ microparticle was purchased from Chongqing Ziyi New Material Technology Co., Ltd. Tetraethoxysilane (TEOS), ammonia ($NH_3{\cdot}H_2O$), 3-aminopropyl triethoxysilane (APTES), and anhydrous ethanol were provided by Sinopharm Chemical Reagent Co., Ltd. Silicone rubber consisting of component A (vinyl silicone oil) and B (hydrogen-containing silicone oil) was obtained from Shenzhen Jipeng Silicon Fluoride Materials Co., Ltd. Karstedt's catalyst and 1-Ethynyl-1-cyclohexanol were supplied by Wuhan Lullaby Pharmaceutical Chemical Co., Ltd.

2.2. Preparation of $In_{51}Bi_{32.5}Sn_{16.5}$@$SiO_2$ microcapsules

Fig. 1a shows the synthesis schematic of the $In_{51}Bi_{32.5}Sn_{16.5}$@$SiO_2$ microcapsules through sol-gel polymerization method. Firstly, 2 g of $In_{51}Bi_{32.5}Sn_{16.5}$ was mixed with 20 ml of anhydrous ethanol in a beaker at room temperature, followed by ultrasonic stirring for 10 min to ensure sufficient dispersion and depolymerization of the microparticles. The treatment was performed in a 20 s cycle for a total of 30 cycles, with 3 s of ultrasonic operation and 17 s of pause. The power of the device is set to 195 W. Secondly, 1 ml of APTES and 1 ml of TEOS were thoroughly mixed with 3 ml deionized water. Thirdly, the two compounds were mixed and stirred on a magnetic stirrer at a stirring rate of 800 rpm for 12 h. Afterwards, 3 ml of $NH_3{\cdot}H_2O$ and 3 ml of deionized water were slowly dropped into the mixture to accelerate the reaction [30,47]. Under alkaline conditions, the hydrolysis rate of TEOS was significantly higher than its condensation rate, resulting in ortho-silicic acid being predominantly formed as the main product. The monomer produced through hydrolysis easily adhered to the surface of alloy microparticle and gradually self-assembled into a silica shell. Finally, $In_{51}Bi_{32.5}Sn_{16.5}$@$SiO_2$ microcapsule powder was obtained through centrifugation and drying.

2.3. Preparation of SR/$In_{51}Bi_{32.5}Sn_{16.5}$@$SiO_2$ composite phase change materials

Fig. 1b shows the preparation process of composite phase change materials. Initially, the SR was synthesized by blending component A and component B at a mass ratio of 4:1. Subsequently, trace amounts of 1-Ethynyl-1-cyclohexanol and Karstedt's catalyst were successively added to the mixture. Then, different volume fractions of $In_{51}Bi_{32.5}Sn_{16.5}$@$SiO_2$ were mixed with the SR through mechanically stirring. Subsequently, the obtained mixtures were transferred into polytetrafluoroethylene (PTFE) molds to shaping in a vacuum environment. Finally, the mixtures were cured at 50 °C for 12 h to obtain a series of SR/$In_{51}Bi_{32.5}Sn_{16.5}$@$SiO_2$ CPCMs named CPCM-1, CPCM-2, CPCM-3, CPCM-4, as shown in Table 1. The pure SR sample was also prepared through the same method for comparison.

2.4. Characterization and measurements

The morphology and microstructure of microcapsules and CPCMs were observed by a field-emission scanning electron microscope (Nova NanoSEM 450, FEI). Energy dispersive spectrometry (EDS) analysis combined with SEM observation was conducted to obtain the elemental mapping of the microcapsules. The cross section elemental distribution of $In_{51}Bi_{32.5}Sn_{16.5}$@$SiO_2$ core-shell structure was analyzed by electron prob. micro-analyzer (EPMA-8050G, SHIMADZU). The thermal stability of the samples was analyzed using a thermogravimetric analyzer (TGA, Netzsch STA 2500). Measurements were made in a nitrogen atmosphere with a temperature range of 20 °C to 700 °C and a heating rate of 5 °C/min. The chemical composition of MEPCM and CPCM were investigated by Fourier transform infrared spectra (FTIR, IRTracer-100) from 4000

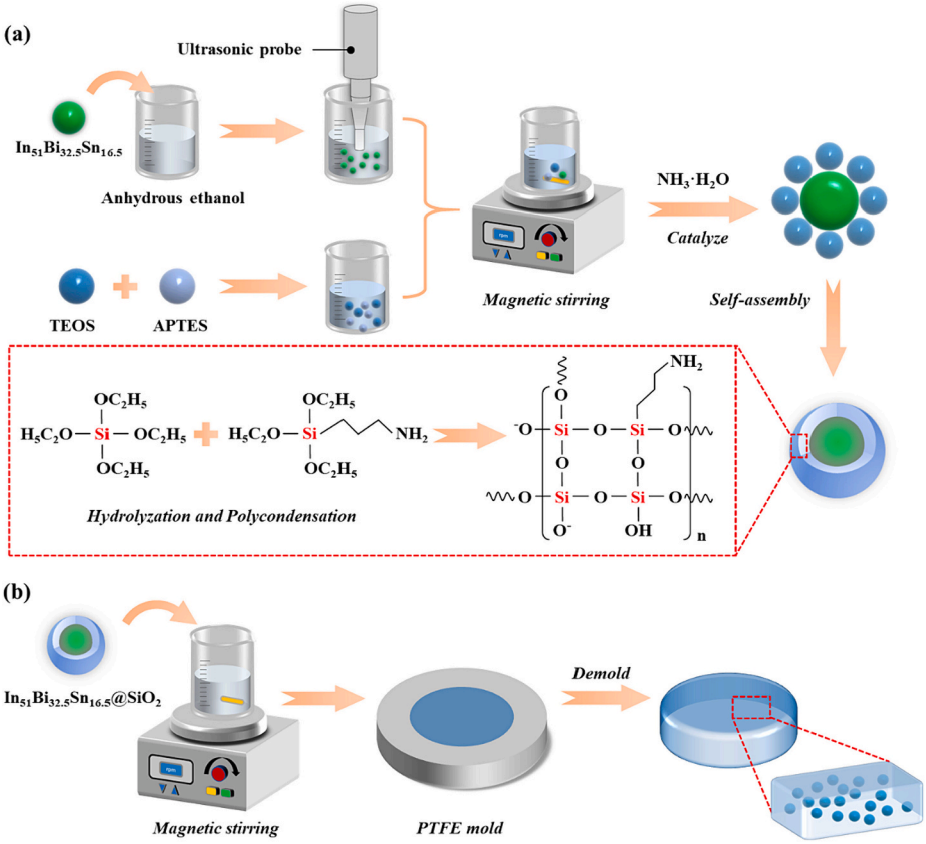

Fig. 1. The preparation process of (a) $In_{51}Bi_{32.5}Sn_{16.5}@SiO_2$ micro-encapsulated phase change material, (b) SR/$In_{51}Bi_{32.5}Sn_{16.5}@SiO_2$ composite phase change material.

Table 1
Sample identification and composition.

Samples	Silicone rubber (vol%)	$In_{51}Bi_{32.5}Sn_{16.5}@SiO_2$ (vol%)
SR	100	0
CPCM-1	90	10
CPCM-2	80	20
CPCM-3	70	30
CPCM-4	60	40

cm^{-1} to 400 cm^{-1}. In addition, the phase change properties of the samples were characterized using a differential scanning calorimeter (Diamond DSC, Perkin Elmer) in nitrogen atmosphere with a heating/cooling rate of 10 °C/min from 45 °C to 80 °C. The thermal conductivities of the composites were measured by laser flash analyzer (LFA 457, Netzsch). To evaluate the performance of CPCMs in chip thermal management, the following devices were employed: a ceramic element (⌀14 mm × 1.3 mm, customizable heat power from Beijing youpu science and Technology Centre) was utilized as the simulated chip, powered by a DC power supply (0–30 V/0–10 A, MS-3010D, Dongguan Maisheng Power Technology Company Ltd). The temperature data was recorded by a data acquisition instrument (MIK-6000F, Hangzhou Meacon Automation Technology Company). Besides, the surface temperature of chip was obtained by the infrared thermograph (SC620, FLIR).

3. Results and discussion

3.1. The morphology and chemical composition of MEPCMs

Fig. 2a–d shows the SEM micrographs of pristine $In_{51}Bi_{32.5}Sn_{16.5}$ alloy particles and $In_{51}Bi_{32.5}Sn_{16.5}@SiO_2$ MEPCMs. The pristine $In_{51}Bi_{32.5}Sn_{16.5}$ present a regular spherical shape with a smooth surface, as illustrated in Fig. 2a and b. On the contrary, a relatively rougher coating layer was observed on the surface of the microcapsules, as shown in Fig. 2c and d, revealing that the $In_{51}Bi_{32.5}Sn_{16.5}$ was well encapsulated through sol-gel polymerization method. Furthermore, statistical analysis reveals that the size distribution of MEPCMs is concentrated within the range of 40–60 μm, with an average of 48.2 ± 6.2 μm. In addition, EDS analysis was conducted to detect the elemental composition of the pristine $In_{51}Bi_{32.5}Sn_{16.5}$ and MEPCMs, as illustrated in Fig. 2f and g. The characteristic peaks of Sn, In and Bi could be observed from Fig. 2g, conforming the chemical components of the PCMs. Furtherly, the characteristic peaks of Si and O elements were probed from the shell in MEPCM, which demonstrates the successful synthesis of the SiO_2 shell. Table 2 shows weight percentage and atomic percentage of each element. The relative percentages of In, Sn, and Bi elements are basically the same before and after encapsulation. The content of Si is 1.98 wt%, which means that the surface of MEPCM is a thin SiO_2 shell.

Fig. 3a shows the structure diagram of samples for elemental distribution analysis of $In_{51}Bi_{32.5}Sn_{16.5}@SiO_2$ core-shell structure. Among them, epoxy resin was chosen for the matrix material to detect the distribution of silicon elements conveniently, and the microcapsules are randomly distributed within the resin matrix material. Fig. 3b–f show the cross-sectional images and elemental distribution of the microcapsule. The MEPCMs are embedded in the resin matrix and meticulously polished to achieve a smooth cross-section surface, as depicted in Fig. 3b. The core-shell structure of microcapsules can be clearly observed from Fig. 3c–f. Notably, there is an accumulation of Si element on the surface of the microcapsule, while elements In, Sn, and Bi are concentrated in the core section surrounded by a circle of Si element wrapping them up together. But they are not forming a single phase, as

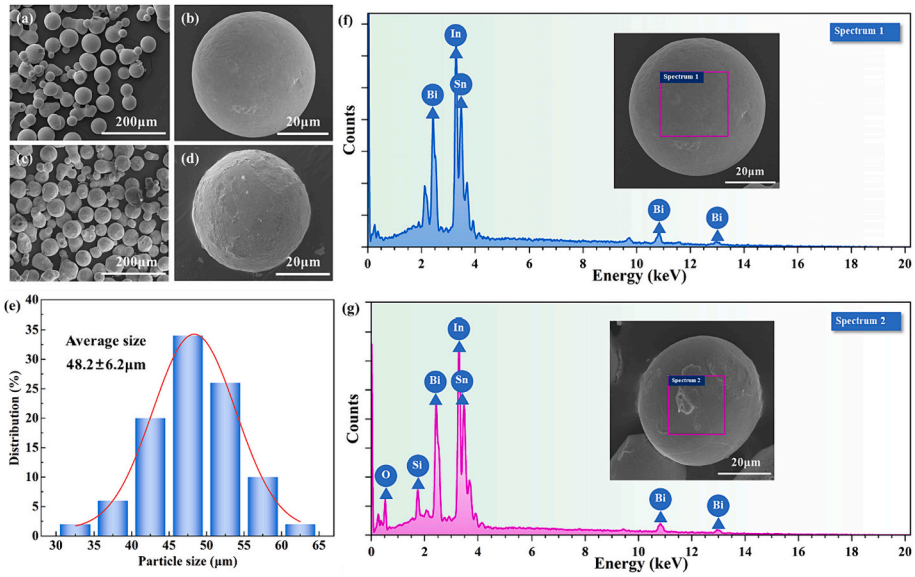

Fig. 2. SEM images of (a-b) $In_{51}Bi_{32.5}Sn_{16.5}$ PCM and (c-d) $In_{51}Bi_{32.5}Sn_{16.5}@SiO_2$ MEPCM, (e) the particle distribution of $In_{51}Bi_{32.5}Sn_{16.5}@SiO_2$ MEPCM, and EDS analysis of (f) $In_{51}Bi_{32.5}Sn_{16.5}$ PCM, (g) $In_{51}Bi_{32.5}Sn_{16.5}@SiO_2$ MEPCM.

Table 2
EDS data of PCM and MEPCM.

Elements	$In_{51}Bi_{32.5}Sn_{16.5}$		$In_{51}Bi_{32.5}Sn_{16.5}@SiO_2$	
	Weight %	Atomic %	Weight %	Atomic %
In	51.54	60.24	41.68	20.74
Bi	30.77	19.76	25.67	7.02
Sn	17.69	20.00	13.37	6.44
O	–	–	17.30	61.77
Si	–	–	1.98	4.03

indicated by their complementary concentration distributions shown in mappings analysis results. Additionally, elemental line analysis from core to surface was conducted to measure shell thickness, revealing that the shell thickness is approximately 4.4 μm according to variation of Si content in Fig. 3h.

Fig. 4 shows the FTIR spectra of SiO_2, $In_{51}Bi_{32.5}Sn_{16.5}$ PCM and $In_{51}Bi_{32.5}Sn_{16.5}@SiO_2$ MEPCM. In the spectrum diagram of SiO_2, the peak at 472 cm^{-1} is the bending vibration of the Si-O-Si bond, while the peaks at 810 cm^{-1} and 1100 cm^{-1} represent the symmetric vibration, and asymmetric vibration of the Si-O-Si bond, respectively [31,36]. There are several small peaks in the spectrum diagram of PCM. It is due to the large specific surface area of the micron-grade alloy material. Therefore, the surface is prone to adsorption of water and oxidation to form oxides, resulting in some absorption peaks. As the reaction proceeds, the hydroxyl sharp peak at 3430 cm^{-1} transforms into a broad peak. The spectrum diagram of MEPCM is composed of that of SiO_2 and PCM, including the most typical 1100 cm^{-1} peak of SiO_2, as well as a merged peak at 900 cm^{-1}. In summary, the FTIR results verify that the surface of the PCM core is wrapped with a shell layer of SiO_2.

3.2. Characterization of phase change microcapsules

The DSC curves of pristine $In_{51}Bi_{32.5}Sn_{16.5}$ and $In_{51}Bi_{32.5}Sn_{16.5}@SiO_2$ microcapsules are presented in Fig. 5. The DSC curves of the microcapsules are similar to that of the pristine PCMs, revealing that the encapsulation shell has no effect on the phase transition characteristics of the $In_{51}Bi_{32.5}Sn_{16.5}$. Table 3 lists the phase change properties of PCM and MEPCM. The melting and freezing peak temperature of $In_{51}Bi_{32.5}Sn_{16.5}$ are 62.5 °C, 57.5 °C, respectively, which exhibits a subcooling of only 5 °C, enabling the immediate release of stored latent heat at the desired temperature to ensure optimal energy utilization. In addition, the melting and freezing enthalpy of $In_{51}Bi_{32.5}Sn_{16.5}$ are 28.98 J/g, and 24.24 J/g, respectively. The microcapsules exhibit a slight reduction in both melting enthalpy and freezing enthalpy compared to pure PCM, with values of 26.83 J/g and 23.15 J/g, respectively, which can be attributed to the formation of the silica shell. The encapsulation ratio (R) and encapsulation efficiency (E) are important parameters to evaluate the heat storage capacity of MEPCMs, which can be calculated by Eqs. (1) and (2) [22,27], respectively.

$$R = \frac{\Delta H_{m,MEPCM}}{\Delta H_{m,PCM}} \times 100\% \quad (1)$$

$$E = \frac{\Delta H_{m,MEPCM} + \Delta H_{c,MEPCM}}{\Delta H_{m,PCM} + \Delta H_{c,PCM}} \times 100\% \quad (2)$$

where $\Delta H_{m,MEPCM}$ and $\Delta H_{c,MEPCM}$ are the melting and freezing enthalpy of MEPCM, respectively. ΔH_m and ΔH_c represent the melting and freezing enthalpy of PCM, respectively. Therefore, the encapsulation ratio and encapsulation efficiency of the MEPCMs could be calculated as 92.6 % and 93.9 %, respectively. In addition, the thermal conductivity of the microcapsules was detected through laser flash method. Firstly, the $In_{51}Bi_{32.5}Sn_{16.5}@SiO_2$ microcapsule powders were pressed into a disk to minimize the contact thermal resistance and interface thermal resistance. Then, the thermal conductivity of the round sheets was tested through laser flash analyzer. The results revealed that the microcapsules exhibited a significant thermal conductivity of 13.49 Wm^{-1} K^{-1} at 25 °C. The exceptional thermal conductivity of these microcapsules enables them to function as highly efficient thermally conductive fillers, establishing an effective network for heat transfer within the matrix.

3.3. Characterization of SR/$In_{51}Bi_{32.5}Sn_{16.5}@SiO_2$ composite phase change materials

Fig. 6a shows the optical images of the pure SR and CPCMs with varying volume fractions of the microcapsules. Pure SR presents a white and transparent appearance, while its color deepens to gray-black as the concentration of microcapsules increases. The cross-sectional morphologies are depicted in Fig. 6b–f. Pure SR presents a smooth section, while CPCMs display rougher profiles due to the presence of embedded microcapsules. It is worth noting that MEPCMs within the SR maintain their complete spherical shape, indicating excellent shape stability. This

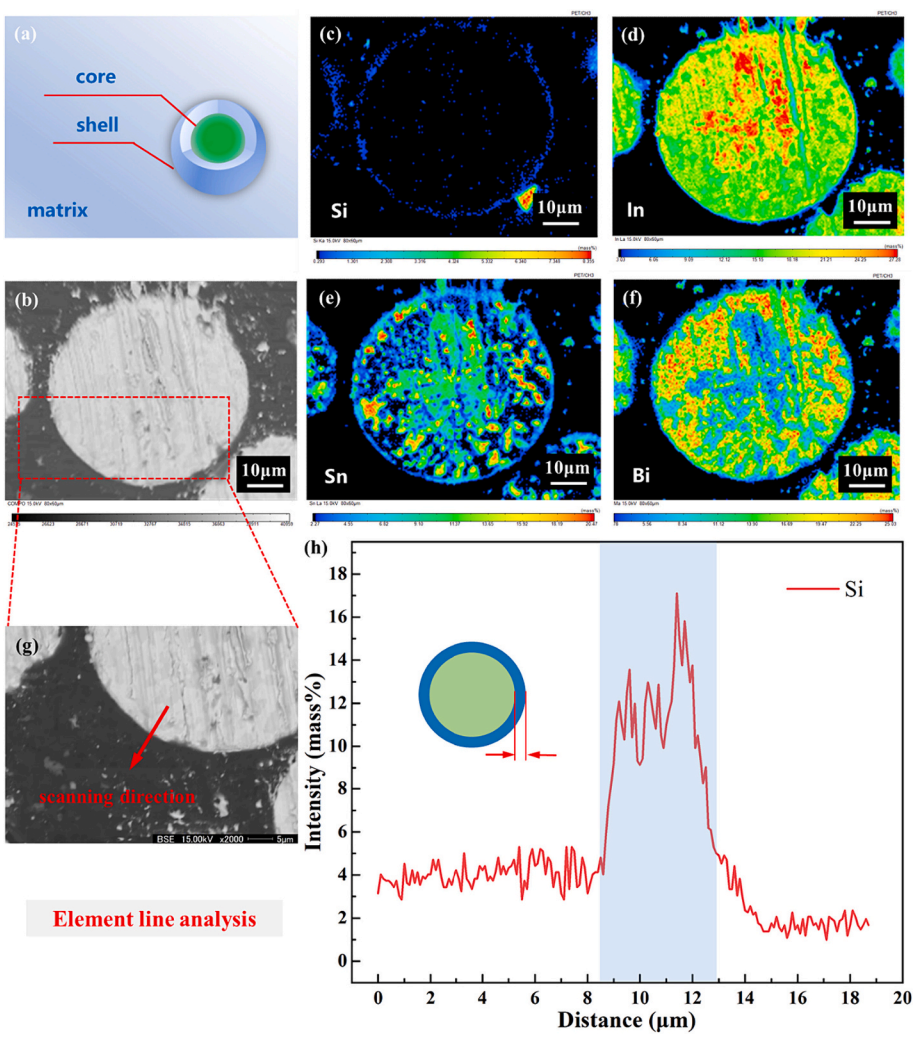

Fig. 3. (a) Structure schematic diagram, (b) cross-sectional image of MEPCM, EPMA mapping of element (c) Si, (d) In, (e) Sn, (f) Bi. And (g) schematic diagram of scanning area and direction, (h) elemental line scan of element Si.

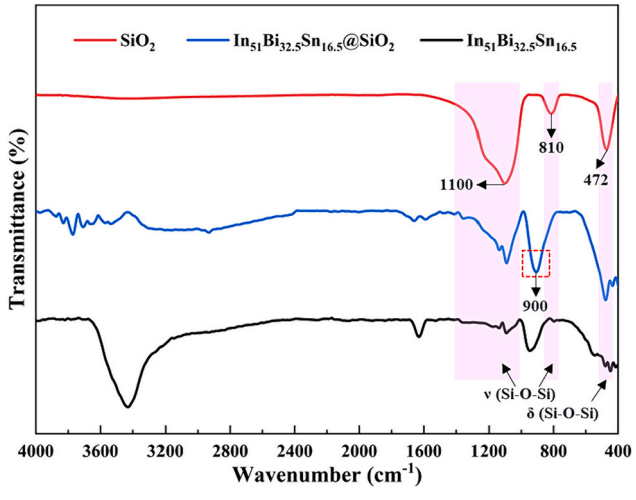

Fig. 4. FTIR spectra of SiO_2, $In_{51}Bi_{32.5}Sn_{16.5}$, and $In_{51}Bi_{32.5}Sn_{16.5}@SiO_2$.

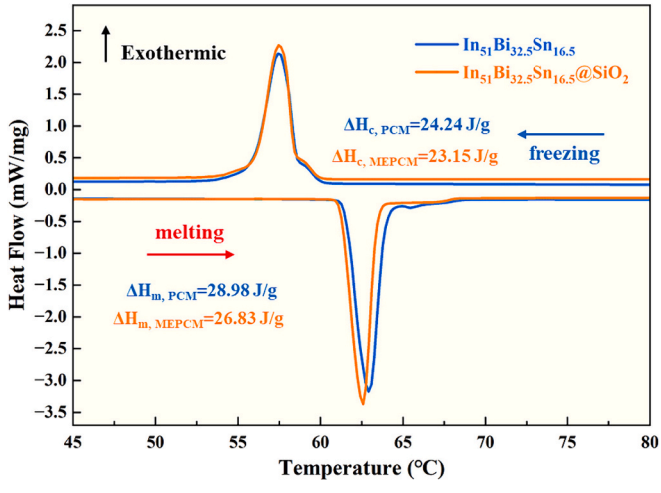

Fig. 5. DSC curves of $In_{51}Bi_{32.5}Sn_{16.5}$ PCM and $In_{51}Bi_{32.5}Sn_{16.5}@SiO_2$ MEPCM.

distribution pattern facilitates the establishment of a thermal conductivity network, particularly for high-filling composites. As illustrated in the Fig. 6b–f, the density of thermal conductivity channels gradually increases with the filling ratio increasing from 0 vol% to 40 vol%.

The DSC curves of CPCMs with different proportions of microcapsules are presented in Fig. 7a–d. The detailed parameters are listed in Table 4. The phase change enthalpy of CPCMs gradually increases with the volume fraction of $In_{51}Bi_{32.5}Sn_{16.5}@SiO_2$ microcapsules. CPCM-4

Table 3
The phase change properties of PCM and MEPCM.

Samples	Melting process		Freezing process	
	T_m (°C)	ΔH_m (J/g)	T_c (°C)	ΔH_c (J/g)
$In_{51}Bi_{32.5}Sn_{16.5}$	61.53	28.98	58.67	24.24
$In_{51}Bi_{32.5}Sn_{16.5}@SiO_2$	61.25	26.83	58.53	23.15

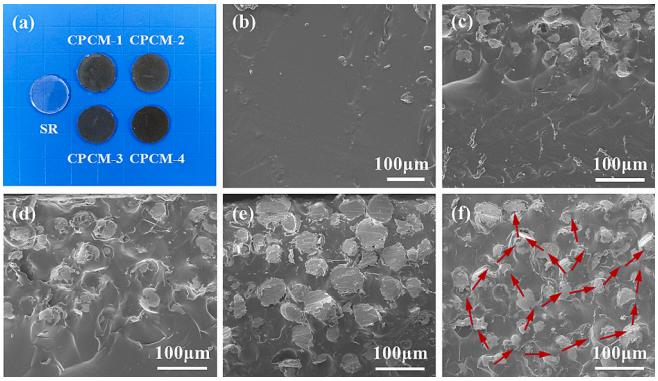

Fig. 6. Photography of the composite phase change materials with different volume fractions of $In_{51}Bi_{32.5}Sn_{16.5}@SiO_2$ microcapsule (a) appearance of all samples, with SEM images of (b) pure SR, (c) CPCM-1, (d) CPCM-2, (e) CPCM-3, (f) CPCM-4.

(40 % volume fraction of microcapsules) exhibits a melting and freezing enthalpy of 21.16 J/g, 18.19 J/g, respectively, which enables them great potential in thermal management. Additionally, Fig. 7e–f illustrates the phase change temperature profiles of both CPCMs and $In_{51}Bi_{32.5}Sn_{16.5}@SiO_2$ microcapsules, where T_m represents the onset temperature for the melting process and T_c denotes the onset temperature for the freezing process. All the samples present almost uniform phase transition temperature, revealing that the composite process with SR has no effect on the phase transition properties of the PCMs.

Fig. 8a illustrates the thermal conductivities of CPCMs with varying volume fractions of microcapsules. For the results of the experiment, the pure SR exhibits an extremely low thermal conductivity of 0.1 $Wm^{-1}K^{-1}$. It is worth noting that the thermal conductivities of the composites gradually increase with the volume fraction of MEPCMs. Notably, CPCM-4 demonstrates the highest thermal conductivity of 0.45 $Wm^{-1}K^{-1}$ among CPCMs, which is significantly increased by 350 % compared to pure SR. This remarkable improvement in CPCM-4 can be attributed to the establishment of efficient thermal channels within the composite structure. Additionally, the Bruggeman model is utilized for theoretical calculation of thermal conductivity, specifically tailored for composite systems with high volume fraction [48,49]. The corresponding equation employed in this specific calculation is as follows:

$$(1-V)^3 = \frac{\lambda_m}{\lambda_c}\left(\frac{\lambda_c-\lambda_f}{\lambda_m-\lambda_f}\right)^3 \quad (3)$$

where V is the volume fraction of thermally conductive filler, λ represents thermal conductivity, and the subscripts m, f, and c mean matrix material, thermally conductive filler, and composite material, respectively. The thermal conductivity was calculated for various volume fractions, as illustrated in Fig. 8a. In comparison, the theoretical calculations and experimental data trends exhibit excellent agreement with an overall average relative error below 10 %, particularly at high volume fractions. In addition, the increase in thermal conductivity of the composites is more significant along with the increase in volume fraction of $In_{51}Bi_{32.5}Sn_{16.5}@SiO_2$. Therefore, the CPCMs composed of $In_{51}Bi_{32.5}Sn_{16.5}@SiO_2$ microcapsules and SR possess high thermal storage capacities and thermal conductivities simultaneously, which is beneficial for the electronic thermal management. Compared to previous studies, the CPCMs prepared in this work exhibit competitive properties as shown in Fig. 8b [50–52]. In particular, $In_{51}Bi_{32.5}Sn_{16.5}@SiO_2$-based CPCMs simultaneously achieved high thermal conductivity with high phase change heat storage density. For CPCM-4, it presents excellent performance with thermal conductivity of 0.45 $Wm^{-1}K^{-1}$ and volume phase change enthalpy of 71.73 J/cm^3.

Fig. 9 shows the photography of appearance and FTIR spectra of CPCM. The shape of the CPCM remains stable before and after 50 thermal cycles. The spectrogram exhibits the primary characteristics of the siloxane group through an asymmetric stretching peak at 1006 cm^{-1}

Table 4
The thermophysical and phase change properties of CPCMs.

Samples	Density (g/cm^3)	Melting process			Freezing process	
		T_m (°C)	ΔH_m (J/g)	$\Delta H_{m,v}$ (J/cm^3)	T_c (°C)	ΔH_c (J/g)
CPCM-1	1.59	61.52	6.82	10.84	58.03	6.03
CPCM-2	2.19	61.58	17.10	37.45	57.98	14.66
CPCM-3	2.79	61.55	19.38	54.07	57.80	16.94
CPCM-4	3.39	61.28	21.16	71.73	58.28	18.19

$\Delta H_{m,v}$ means phase change enthalpy per unit volume of the CPCMs.

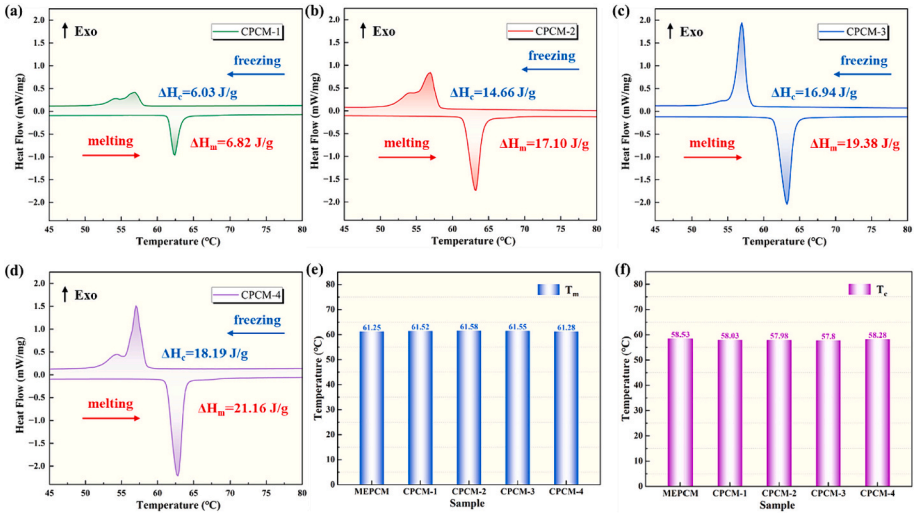

Fig. 7. DSC curves of (a) CPCM-1, (b) CPCM-2, (c) CPCM-3, (d) CPCM-4, (e) the melting point of MEPCM and CPCMs, (f) the freezing point of MEPCM and CPCMs.

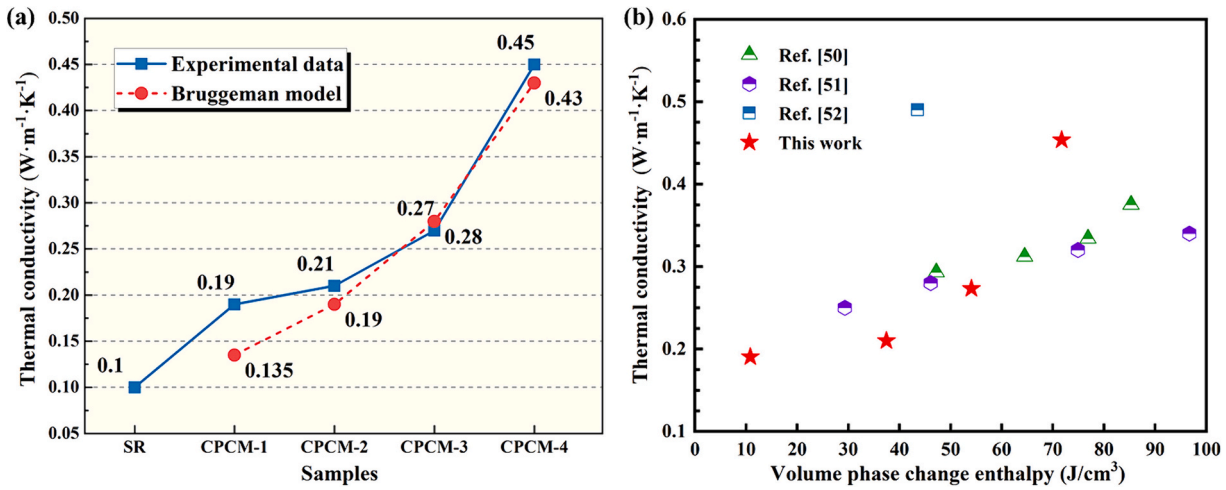

Fig. 8. (a) Comparison of experimental data with theoretical calculation data of CPCMs, (b) comparison with other representative studies on microcapsules based CPCMs.

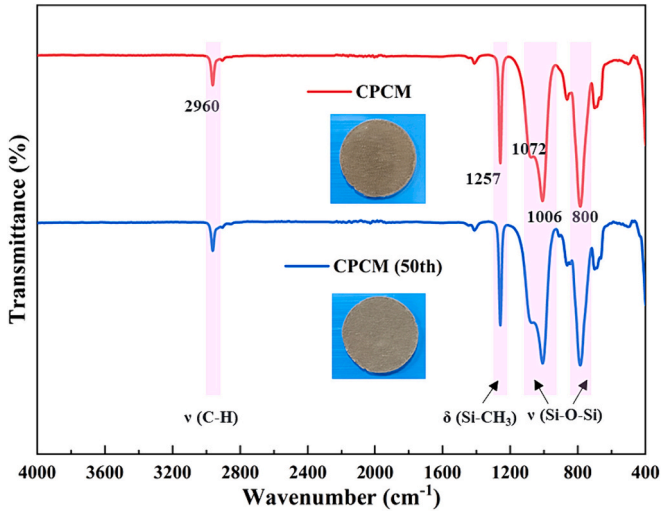

Fig. 9. Photography of appearance and FTIR spectra of CPCM before and after 50 thermal cycles.

and a symmetrical stretching peak at 800 cm^{-1} [27,29]. In the range of 1000 cm^{-1} to 1200 cm^{-1}, the characteristic peaks of Si-O-Si of silicone rubber and SiO_2 are superimposed, as evidenced by a broader peak. The absorption peak observed at 2960 cm^{-1} corresponds to the stretching vibration of the C—H bond, while the peak at 1257 cm^{-1} is indicative of the bending vibration associated with the Si-CH_3 group. Upon comparison before and after cycling, the primary characteristic peaks remained unaltered, indicating that CPCM developed in this study exhibits favorable chemical stability.

Fig. 10a–b illustrate the thermogravimetric curves of PCM, MEPCM, and CPCM. With the increasing of temperature, the mass of alloy PCM and MEPCM have no obvious changes, showing excellent thermal stability. In particular, the mass is almost constant in the interval less than 200 °C in Fig. 10b, which is favorable for practical applications in thermal management of electronic devices. And in the high temperature range of 200 °C to 700 °C, the mass begins to increase slowly due to the presence of trace amounts of oxygen in the nitrogen. Compared to pure PCM, MEPCM still maintains mass stability at 400 °C due to the protective effect of the SiO_2 shell, with a weight increase of only 0.09 %. In Fig. 10a, CPCM-2 shows a 1.66 % mass reduction in the range of 20 °C to 100 °C because of the evaporation of the residual water. Subsequently, the mass decreases by only 0.56 % in the interval from 100 °C to 250 °C.

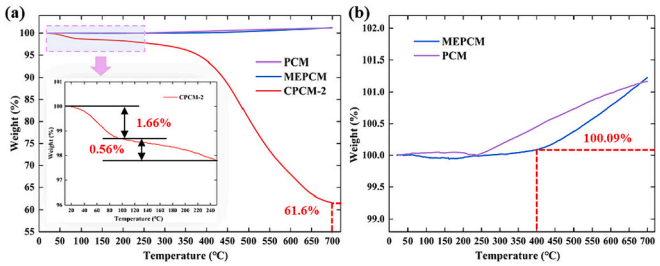

Fig. 10. Thermogravimetric curves of (a) all samples, (b) comparison between PCM and MEPCM.

And the overall mass of CPCM-2 continues to decrease after further heating due to the decomposition of the organic silicone at high temperature. The silicone rubber decomposes rapidly after 300 °C and the sample stabilizes at 700 °C with mass of 61.6 %.

3.4. Application of the composites in chip thermal management

To evaluate the thermal management performance of CPCMs in thermal management of chip, a testing system was designed as shown in Fig. 11a. Specifically, both pure SR and CPCMs were assembled between the simulated chip and the constant temperature plate of 20 °C. A data acquisition device monitors the upper surface temperature of the chip during a heating period of 240 s. Fig. 11b shows the results of test samples at 1.6 W heating power. As the volume fraction of phase change microcapsules increased, the temperature rise rate of the chip gradually slows down. After heating for 240 s, the temperature of chip with pure SR reaches 97.1 °C, while chips employing CPCMs exhibited significantly lower temperatures. Notably, CPCM-4 demonstrated superior temperature control performance with a final temperature of 73.6 °C, representing a reduction of 24 % compared to pure SR, indicating that the prepared CPCMs effectively delay the temperature rise of the chip on account of the high phase change enthalpy and thermal conductivity. Fig. 11c illustrates the infrared images of the chip at the final moment. It is evident that introducing CPCM-4 leads to significantly lower temperatures on the simulated chip surface compared to other cases without CPCMs present. Overall, the CPCMs exhibit excellent heat transfer performance and their promising potential within thermal management applications.

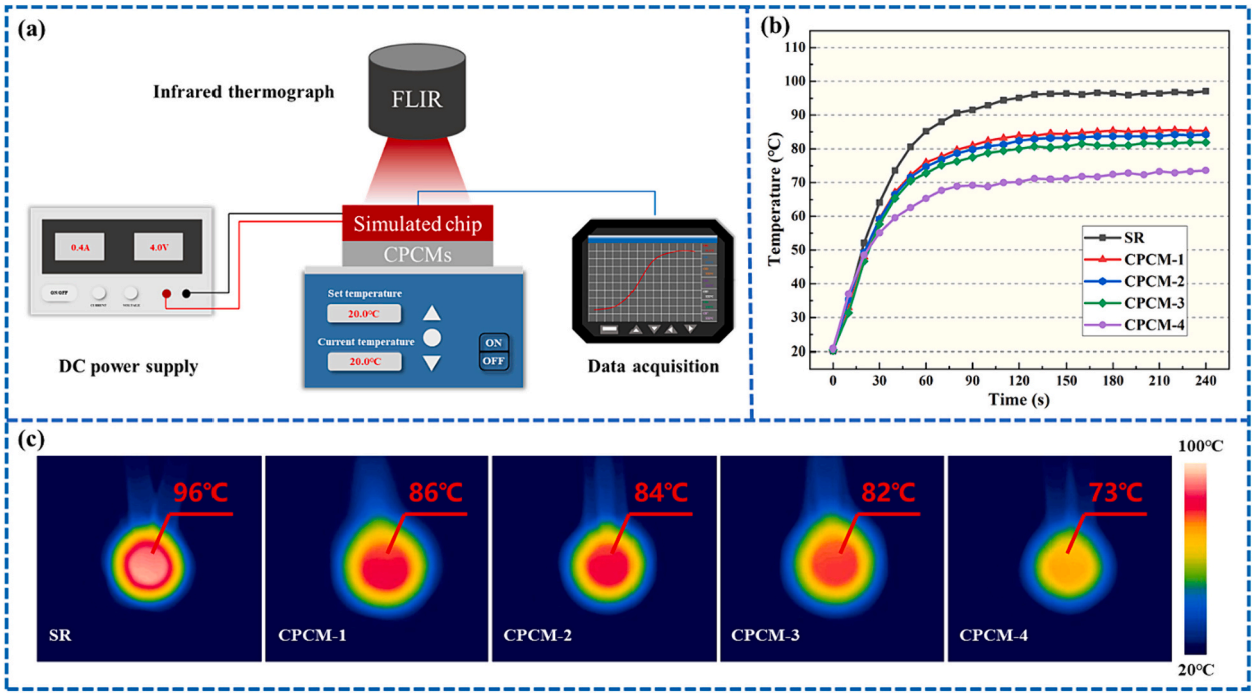

Fig. 11. (a) Schematic diagram of experimental set-up, (b) Curves of simulated chip surface temperature with time, (c) Infrared thermal images of pure SR and CPCMs at 240 s.

4. Conclusions

In this study, $In_{51}Bi_{32.5}Sn_{16.5}$@$SiO_2$ MEPCMs were synthesized through the sol-gel polymerization method. The microstructures and chemical composition of the MEPCMs were detected and proved by the test of SEM, EDS, EPMA and FTIR. Furtherly, CPCMs consisting of $In_{51}Bi_{32.5}Sn_{16.5}$@$SiO_2$ MEPCMs and SR matrix were prepared through vacuum template method. The enthalpy of the CPCMs can reach as high as 21.16 J/g and 71.73 J/cm^3 with 40 % of MEPCMs loading. Notably, the thermal conductivity of the CPCMs was increased to 0.45 Wm^{-1} K^{-1}, representing a remarkable 350 % improvement compared to pure SR. Furthermore, a series of CPCMs were applied to thermal management of chip. Among them, CPCM-4 exhibits a 24 % reduction in chip temperature compared to pure SR, resulting in a remarkable decrease of 23 °C. Consequently, the utilization of CPCMs holds great promise in the field of electronic thermal management due to their exceptional thermal conductivity, adjustable thermal energy storage capacity, and thermal stability.

CRediT authorship contribution statement

Chao Deng: Writing – original draft, Methodology, Investigation, Conceptualization. **Xinfeng Zhang:** Methodology, Data curation. **Jiale Peng:** Validation, Formal analysis. **Xuan Yang:** Formal analysis, Data curation. **Bofeng Shang:** Writing – review & editing, Methodology, Funding acquisition. **Xiaobing Luo:** Writing – review & editing, Supervision, Funding acquisition, Conceptualization.

Declaration of competing interest

The authors declare that they have no known competing financial interests or personal relationships that could have appeared to influence the work reported in this paper.

Data availability

Data will be made available on request.

Acknowledgements

This research was supported by the Open Fund Science and Technology on Thermal Energy and Power Laboratory (No. TPL2022B02), and the Natural Science Foundation of Henan Province (Grant No. 222300420310).

References

[1] R. van Erp, R. Soleimanzadeh, L. Nela, G. Kampitsis, E. Matioli, Co-designing electronics with microfluidics for more sustainable cooling, Nature 585 (2020) 211–216.
[2] Q. Yan, F.E. Alam, J. Gao, W. Dai, X. Tan, J. Le Lv, H. Wang, D. Zhang, K. Chen, L. Nishimura, J. Wang, J. Yu, R. Lu, R. Sun, S. Xiang, H. Maruyama, S. Zhang, N. Wu, C. Lin Jiang, Soft and self-adhesive thermal interface materials based on vertically aligned, covalently bonded graphene nanowalls for efficient microelectronic cooling, Adv. Funct. Mater. 31 (36) (2021) 2104062.
[3] B. Hu, W. Zhang, H. Guo, S. Xu, Y. Li, M. Li, B. Li, Nacre-mimetic elastomer composites with synergistic alignments of boron nitride/graphene oxide towards high through-plane thermal conductivity, Compos. Part a.-Appl. S. 156 (2022) 106891.
[4] Z. Ling, Z. Zhang, G. Shi, X. Fang, L. Wang, X. Gao, Y. Fang, T. Xu, S. Wang, X. Liu, Review on thermal management systems using phase change materials for electronic components, Li-ion batteries and photovoltaic modules, Renew. Sustain. Energy Rev. 31 (2014) 427–438.
[5] J. Peng, W. Lan, F. Wei, C. Deng, B. Xie, X. Luo, A numerical model coupling multiple heat transfer modes to develop a passive thermal management system for logging tool, Appl. Therm. Eng. 223 (2023) 120011.
[6] A.R.M. Siddique, S. Mahmud, B. Van Heyst, A comprehensive review on a passive (phase change materials) and an active (thermoelectric cooler) battery thermal management system and their limitations, J. Power Sources 401 (2018) 224–237.
[7] H. Zhang, C.L. Xu, G.Y. Fang, Encapsulation of inorganic phase change thermal storage materials and its effect on thermophysical properties: a review, Sol. Energ. Mat. Sol. C. 241 (2022) 111747.
[8] G. Wang, Z. Tang, Y. Gao, P. Liu, Y. Li, A. Li, X. Chen, Phase change thermal storage materials for interdisciplinary applications, Chem. Rev. 123 (2023) 6953–7024.
[9] W. Lan, J. Zhang, J. Peng, Y. Ma, S. Zhou, X. Luo, Distributed thermal management system for downhole electronics at high temperature, Appl. Therm. Eng. 180 (2020) 115853.
[10] S. Gong, X.X. Sheng, X.L. Li, M.J. Sheng, H. Wu, X. Lu, J.P. Qu, A multifunctional flexible composite film with excellent multi-source driven thermal management, electromagnetic interference shielding, and fire safety performance, inspired by a "brick-mortar" sandwich structure, Adv. Funct. Mater. 32 (26) (2022) 2200570.
[11] H. Koide, A. Kurniawan, T. Takahashi, T. Kawaguchi, H. Sakai, Y. Sato, J.N. Chiu, T. Nomura, Performance analysis of packed bed latent heat storage system for

high-temperature thermal energy storage using pellets composed of micro-encapsulated phase change material, Energy 238 (2022) 121746.
[12] F.S. Javadi, H.S.C. Metselaar, P. Ganesan, Performance improvement of solar thermal systems integrated with phase change materials (PCM), a review, Sol. Energy 206 (2020) 330–352.
[13] S.P. Yuan, R. Yan, B.B. Ren, Z.L. Du, X. Cheng, X.S. Du, H.B. Wang, Robust, double-layered phase-changing microcapsules with superior solar-thermal conversion capability and extremely high energy storage density for efficient solar energy storage, renew, Energ 180 (2021) 725–733.
[14] K.J. Yuan, J.M. Shi, W. Aftab, M.L. Qin, A. Usman, F. Zhou, Y. Lv, S. Gao, R.Q. Zou, Engineering the thermal conductivity of functional phase-change materials for heat energy conversion, storage, and utilization, Adv. Funct. Mater. 30 (8) (2020) 1904228.
[15] M.Q. Wu, S. Wu, Y.F. Cai, R.Z. Wang, T.X. Li, Form-stable phase change composites: preparation, performance, and applications for thermal energy conversion, storage and management, Energy Storage Mater 42 (2021) 380–417.
[16] Y. Liu, R. Zheng, J. Li, High latent heat phase change materials (PCMs) with low melting temperature for thermal management and storage of electronic devices and power batteries: critical review, Renew. Sustain. Energy Rev. 168 (2022) 112783.
[17] X. Lu, B. Liang, X. Sheng, T. Yuan, J. Qu, Enhanced thermal conductivity of polyurethane/wood powder composite phase change materials via incorporating low loading of graphene oxide nanosheets for solar thermal energy storage, Sol. Energ. Mat. Sol. C. 208 (2020) 110391.
[18] H. Hu, Recent advances of polymeric phase change composites for flexible electronics and thermal energy storage system, Compos. Part B-Eng. 195 (2020) 108094.
[19] J. Bao, D. Zou, S. Zhu, Q. Ma, Y. Wang, Y. Hu, A medium-temperature, metal-based, microencapsulated phase change material with a void for thermal expansion, Chem. Eng. J. 415 (2021) 128965.
[20] B. Shang, R. Wu, J. Hu, R. Hu, X. Luo, Non-monotonously tuning thermal conductivity of graphite-nanosheets/paraffin composite by ultrasonic exfoliation, Int. J. Therm. Sci. 131 (2018) 20–26.
[21] J. Lu, N. Sheng, C. Zhu, Fabrication of Sn@SiO_2 core-shell microcapsules with high durability for medium-temperature thermal energy storage, Sol. Energ. Mat. Sol. C. 239 (2022) 111652.
[22] H. Liu, X.D. Wang, D.Z. Wu, Innovative design of microencapsulated phase change materials for thermal energy storage and versatile applications: a review, Sustain Energ Fuels 3 (5) (2019) 1091–1149.
[23] Q. Zhao, F. He, Q. Zhang, J. Fan, R. He, K. Zhang, H. Yan, W. Yang, Microencapsulated phase change materials based on graphene Pickering emulsion for light-to-thermal energy conversion and management, Sol. Energ. Mat. Sol. C. 203 (2019) 110204.
[24] Y. Konuklu, H.Ö. Paksoy, Polystyrene-based caprylic acid microencapsulation for thermal energy storage, Sol. Energ. Mat. Sol. C. 159 (2017) 235–242.
[25] M. Graham, E. Shchukina, P.F. De Castro, D. Shchukin, Nanocapsules containing salt hydrate phase change materials for thermal energy storage, J. Mater. Chem. A 4 (43) (2016) 16906–16912.
[26] H. Liu, J. Niu, X. Wang, D. Wu, Design and construction of mesoporous silica/n-eicosane phase-change nanocomposites for supercooling depression and heat transfer enhancement, Energy 188 (2019) 116075.
[27] Z. Sun, K. Sun, H.Z. Zhang, H. Liu, D.Z. Wu, X.D. Wang, Development of poly (ethylene glycol)/silica phase-change microcapsules with well-defined core-shell structure for reliable and durable heat energy storage, Sol. Energ. Mat. Sol. C. 225 (2021) 111069.
[28] S. Zhu, D. Zou, J. Bao, Q. Ma, Y. Wang, Y. Hu, Synthesis and characterization of a novel high durability alloy microcapsule for thermal energy storage, Sol. Energ. Mat. Sol. C. 230 (2021) 111262.
[29] H.H. Liao, S.W. Guo, Y. Liu, Q. Wang, Form-stable phase change composites with high thermal conductivity and adjustable thermal management capacity, Sol. Energ. Mat. Sol. C. 221 (2021) 110881.
[30] H. Deng, Y.M. Yang, X.H. Tang, Y.S. Li, F.F. He, Q.P. Zhang, Z. Huang, Z.J. Yang, W.B. Yang, Phase-change composites composed of silicone rubber and pa@SiO_2@PDA double-shelled microcapsules with low leakage rate and improved mechanical strength, ACS Appl Mater Inter 13 (33) (2021) 39394–39403.
[31] Y. Zhou, S. Li, Y. Zhao, Z. Ling, Z. Zhang, X. Fang, Compatible paraffin@SiO_2 microcapsules/polydimethylsiloxane composites with heat storage capacity and enhanced thermal conductivity for thermal management, Compos. Sci. Technol. 218 (2022) 109192.
[32] Y.Q. Ma, H.C. Wang, L. Zhang, X.X. Sheng, Y. Chen, Flexible phase change composite films with improved thermal conductivity and superb thermal reliability for electronic chip thermal management, Compos. Part a.-Appl. S. 163 (2022) 107203.
[33] X. Zhu, X. Li, J. Shen, B. Wang, Z. Mao, H. Xu, X. Feng, X. Sui, Stable microencapsulated phase change materials with ultrahigh payload for efficient cooling of mobile electronic devices, Energ. Convers. Manage. 223 (2020) 113478.
[34] Z. Ling, F. Wang, X. Fang, X. Gao, Z. Zhang, A hybrid thermal management system for lithium ion batteries combining phase change materials with forced-air cooling, Appl. Energ. 148 (2015) 403–409.
[35] S. Wu, T.X. Li, M.Q. Wu, J.X. Xu, Y.H. Hu, J.W. Chao, T.S. Yan, R.Z. Wang, Highly thermally conductive and flexible phase change composites enabled by polymer/graphite nanoplatelet-based dual networks for efficient thermal management, J. Mater. Chem. A 8 (38) (2020) 20011–20020.
[36] L. Kang, L.C. Ren, H.Y. Niu, R.C. Lv, H.C. Guo, S.L. Bai, Paraffin@SiO_2 microcapsules-based phase change composites with enhanced thermal conductivity for passive battery cooling, Compos. Sci. Technol. 230 (2022) 109756.
[37] M.J. Song, F.X. Niu, N. Mao, Y.X. Hu, S.M. Deng, Review on building energy performance improvement using phase change materials, Energ, Buildings 158 (2018) 776–793.
[38] K.O. Lee, M.A. Medina, X. Sun, X. Jin, Thermal performance of phase change materials (PCM)-enhanced cellulose insulation in passive solar residential building walls, Sol. Energy 163 (2018) 113–121.
[39] Y. Peng, Y. Cui, Advanced textiles for personal thermal management and energy, Joule 4 (4) (2020) 724–742.
[40] Y. Lu, X. Xiao, J. Fu, C. Huan, S. Qi, Y. Zhan, Y. Zhu, G. Xu, Novel smart textile with phase change materials encapsulated core-sheath structure fabricated by coaxial electrospinning, Chem. Eng. J. 355 (2019) 532–539.
[41] J. Wang, J. Xu, Y. He, Novel smart textile with ultraviolet shielding and thermo-regulation fabricated via electrospinning, J. Energy Storage 42 (2021) 103094.
[42] K.J. Yuan, H.C. Wang, J. Liu, X.M. Fang, Z.G. Zhang, Novel slurry containing graphene oxide-grafted microencapsulated phase change material with enhanced thermo-physical properties and photo-thermal performance, Sol. Energ. Mat. Sol. C. 143 (2015) 29–37.
[43] J. Feng, Z.J. Liu, D.Q. Zhang, Z. He, Z.C. Tao, Q.G. Guo, Phase change materials coated with modified graphene-oxide as fillers for silicone rubber used in thermal interface applications, New Carbon Mater. 34 (2) (2019) 188–195.
[44] S. Wang, K. Lei, Z.Y. Wang, H. Wang, D.Q. Zou, Metal-based phase change material (PCM) microcapsules/nanocapsules: fabrication, thermophysical characterization and application, Chem. Eng. J. 438 (2022) 135559.
[45] Y. Lin, G. Alva, G. Fang, Review on thermal performances and applications of thermal energy storage systems with inorganic phase change materials, Energy 165 (2018) 685–708.
[46] S.C. Costa, M. Kenisarin, A review of metallic materials for latent heat thermal energy storage: Thermophysical properties, applications, and challenges, Renew. Sustain. Energy Rev. 154 (2022) 111812.
[47] Y. Fang, L. Huang, X. Liang, S. Wang, H. Wei, X. Gao, Z. Zhang, Facilitated synthesis and thermal performances of novel SiO_2 coating $Na_2HPO_4{\cdot}7H_2O$ microcapsule as phase change material for thermal energy storage, Sol. Energ. Mat. Sol. C. 206 (2020) 110257.
[48] Y. Agari, T. Uno, Estimation on thermal conductivities of filled polymers, J. Appl. Polym. Sci. 32 (7) (1986) 5705–5712.
[49] H.J. OTT, Thermal conductivity of composite materials, Rubber Process 1 (1981) 9–11.
[50] X. Liu, T. Cai, S. Jiang, Z. Jiang, F. He, Y. Li, R. He, K. Zhang, W. Yang, Experimental study and numerical simulation of heat transfer behavior based on silicone rubber/paraffin @SiO_2 shape-stabilized phase change material, J. Energy Storage 44 (2021) 103431.
[51] Z. Zhou, Y. Zhao, Z. Ling, Z. Zhang, W. Lin, X. Fang, Simulative study on the performance of polymeric composites containing phase change capsules for chip heat dissipation, J. Energy Storage 68 (2023) 107851.
[52] L. Xu, K. Zhang, R. He, A. Yang, L. Su, Y. Li, F. He, S. Jiang, W. Yang, Phase change composites based on double-shell microcapsules with high latent heat and low leakage rate for thermal energy storage and temperature regulation, J. Energy Storage 55 (2022) 105428.